ACS Energy LETTERS

Cite This: ACS Energy Lett. 2018, 3, 1360−1365

LETTER

Evaluating the Stability of Co_2P Electrocatalysts in the Hydrogen Evolution Reaction for Both Acidic and Alkaline Electrolytes

Yue Zhang,[†] Lu Gao,[†] Emiel J. M. Hensen,*[] and Jan P. Hofmann*[]

Laboratory of Inorganic Materials Chemistry, Department of Chemical Engineering and Chemistry, Eindhoven University of Technology, P.O. Box 513, 5600MB Eindhoven, The Netherlands

Supporting Information

ABSTRACT: The evaluation of the stability of emerging earth-abundant metal phosphide electrocatalysts by solely electrochemical current−potential sweeps is often not conclusive. In this study, we investigated Co_2P to evaluate its stability under both acidic (0.5 M H_2SO_4) and alkaline (1.0 M KOH) hydrogen evolution (HER) conditions. We found that the electrochemical surface area (ECSA) of Co_2P only slightly increased in acidic conditions but almost doubled after electrolysis in alkaline electrolyte. The surface composition of the electrode remained almost unchanged in acid but was significantly altered in alkaline during current−potential sweeps. Analysis of the electrolytes after the stability test shows almost stoichiometric composition of Co and P in acid, but a preferential dissolution of P over Co could be observed in alkaline electrolyte. Applying comprehensive postcatalysis analysis of both the electrode and electrolyte, we conclude that Co_2P, prepared by thermal phosphidization, dissolves stoichiometrically in acid and degrades to hydroxides under alkaline stability testing.

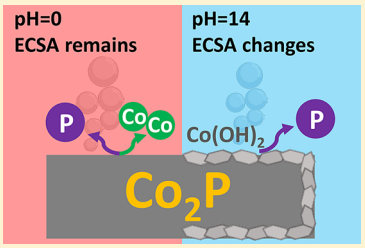

The development of clean, renewable, and affordable energy is a global challenge nowadays. It has been recognized that extensive use of fossil fuels is not suitable to base a sustainable society on. Solar, wind, and other green energy sources are considered as promising alternatives to the conventional fossil energy source. However, those sources are often highly intermittent. Thus, large-scale energy storage is crucial for achieving practical renewable electricity-to-grid integration.

Hydrogen is regarded as the ideal energy carrier because of its high gravimetric energy density and its clean combustion product. Currently, H_2 is mainly obtained through steam reforming of methane, which still consumes fossil fuels and emits CO_2. An alternative renewable way to produce hydrogen is water electrolysis, where hydrogen is produced at the cathode and oxygen at the anode. Although platinum is the best-performing and best-studied catalyst for the hydrogen evolution reaction (HER), the scarcity and high cost of Pt limit its large-scale application. The search for earth-abundant, noncritical electrocatalysts to replace Pt has triggered significant research efforts. A range of transition metal-based materials such as metal chalcogenides, selenides, carbides, and phosphides as well as their alloys has emerged as earth-abundant electrocatalysts for HER in either acidic or alkaline in recent years.[1−5] Among them, transition metal phosphides (TMPs), including nickel phosphides,[6−8] cobalt phosphides,[9−17] iron phosphides,[18−20] molybdenum phosphides,[21−23] tungsten phosphides,[24,25] copper phosphides,[26] and their alloys[27−29] have been discovered to be active in HER electrocatalysis. Nonetheless, little work has systematically studied the stability of these earth-abundant electrocatalysts, and the degradation mechanisms are still ambiguous.[30]

Most TMPs are claimed stable based on electrochemical stability tests such as repeated linear/cyclic voltammetry or chronoamperometry/chronopotentiometry. However, postelectrolysis analysis typically shows significant compositional, structural, and morphological changes. For example, TMPs synthesized by thermal phosphidization showed an apparent electrochemical stability along with distinct compositional changes.[31]

Here, we used cobalt phosphide (Co_2P) prepared by thermal phosphidization as a model electrocatalyst to elucidate its decomposition mechanism during electrochemical stability testing. We investigated the stabilities in both acid and alkaline electrolytes and compared the structural, compositional, and morphological changes induced by the stability tests. Our results show that Co_2P is stable in neither acidic nor alkaline electrolytes and that the degradation mechanism is pH-dependent. While Co_2P stoichiometrically dissolves in acid, it

Received: March 29, 2018
Accepted: May 16, 2018
Published: May 16, 2018

DOI: 10.1021/acsenergylett.8b00514
ACS Energy Lett. 2018, 3, 1360−1365

tends to form hydroxides under alkaline electrolysis conditions. Interestingly, the observed apparent electrochemical stability of Co_2P in alkaline is attributed to the increased electrochemical surface area (ECSA). From our studies, we emphasize the importance of postcatalysis structural and compositional analysis of both the electrode and electrolyte to characterize the intrinsic stability of earth-abundant electrocatalysts.

Thermally phosphidized cobalt phosphide on carbon paper (CP) was assessed by XRD to verify its crystal phase composition. The X-ray diffractogram of the as-synthesized electrode (Figure S1, black line) shows the pattern of Co_2P. The diffraction peaks at 2θ = 40.8, 43.3, 48.7, 50.3, and 52.1° are indexed to the (121), (211), (031), (310), and (002) planes of Co_2P (PDF No.: 00-032-0306), respectively. The Raman spectrum of the as-synthesized Co_2P sample (Figure S2, black line) is consistent with literature.[14,32]

The activities and stabilities of Co_2P@CP in both acidic (0.5 M H_2SO_4) and alkaline (1 M KOH) solutions are shown in Figure 1. The currents are normalized to the geometric surface

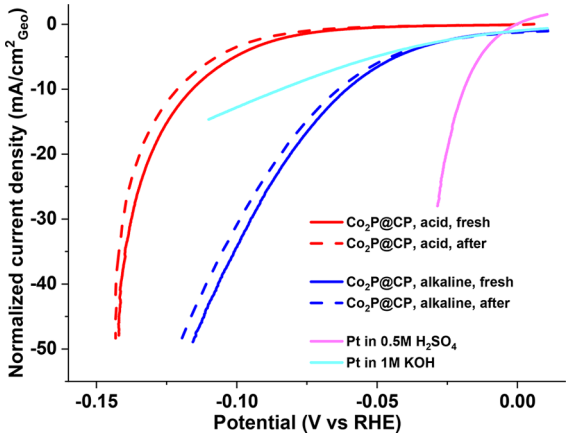

Figure 1. Polarization curves (normalized by geometric area) with 2 mV/s of Co_2P@CP before (solid lines) and after 2000 LSV sweeps (dashed lines) and the Pt rotating disk electrode as the reference (1600 rpm) in 0.5 M H_2SO_4 and 1 M KOH.

area of the electrodes. Co_2P@CP shows excellent catalytic activity in both acidic and alkaline electrolytes (red and blue solid lines) and reaches geometric current densities of 10 mA/cm^2 at overpotentials of only ca. 0.12 and 0.07 V, respectively. The activity of a Pt disk electrode is also shown for comparison. After 2000 LSV sweeps, the geometric current densities of Co_2P@CP barely change in both acidic and alkaline electrolytes (red and blue dashed lines in Figure 2a). No bulk phase change of Co_2P could be observed by XRD after stability tests in both acidic and alkaline conditions (Figure S1, red and blue solid lines), as further corroborated by Raman spectroscopy (Figure S2, red and blue solid lines). On the basis of this data, we can draw the preliminary conclusion that Co_2P is an active and stable electrocatalyst for HER in both acid and alkaline solutions, in accordance with recently published research.[12,27,33]

SEM images of fresh Co_2P@CP (Figure 2a) show nanostructured surface features with a particle size of 120 ± 30 nm. EDX analysis of the fresh sample (Figure 2d, black line) indicates that the bulk composition ratio of Co to P is 2.0 ± 0.1, which is consistent with the phase of Co_2P (XRD, Raman). After stability tests in acidic and alkaline solutions (Figure 2b,c), the overall morphology barely changed. However, the higher-magnification SEM image (inset of Figure 2c) shows a

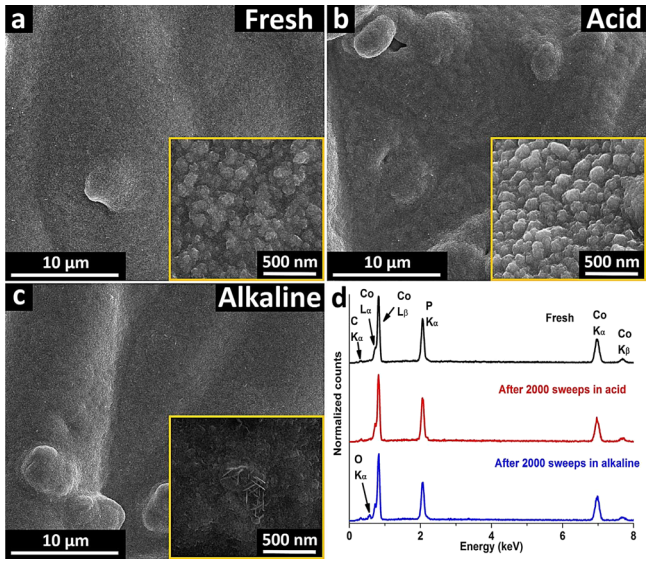

Figure 2. SEM images of (a) as-synthesized Co_2P@CP, (b) Co_2P@CP after stability test in acid, and (c) Co_2P@CP after stability test in alkaline and (d) EDX spectra of Co_2P@CP before and after stability tests.

more flake-shaped nanostructure after stability testing in alkali, which resembles the SEM morphology of cobalt oxides or hydroxide.[34] EDX analysis after 2000 LSV sweeps shows that the composition ratio of Co to P decreased to 1.8 ± 0.1 in acid (Figure 2d, red spectrum and Table S1 in the Supporting Information), indicating Co leaching from the film during the stability test. On the contrary, the composition ratio of Co to P increased to 2.2 ± 0.1 in alkaline (Figure 2d, blue line), meaning that P was leached from the film during the stability test.

The evident compositional changes of the Co_2P@CP were further analyzed by X-ray photoelectron spectroscopy (XPS). As shown in Figure 3a, the Co 2p spectra of the fresh sample (black solid line) reveal a dominant component at BE(Co $2p_{3/2}$) = 778.9 eV, corresponding to $Co^{\delta+}$ ($0 < \delta < 1$)[35,36] covalently bound to P in cobalt phosphide Co_2P.[27,37] The shoulder at higher binding energy (780.6 eV) is attributed to the asymmetric plasmon loss of metal phosphides[27,35] and possible cobalt oxide species as a result of sample exposure to air.[34,38,39] After stability testing in acid, the Co $2p_{3/2}$ peaks remain almost unchanged. In contrast, significant changes are observed after the stability test in alkaline electrolyte: the peak assigned to $Co^{\delta+}$ decreases substantially, while the intensity of the component at BE(Co $2p_{3/2}$) = 780.6 eV assigned to oxidic Co increases. Meanwhile, two new peaks at BE(Co $2p_{3/2}$) = 782.1 and 786.3 eV appear. Although the peak at 782.1 eV has been reported to appear in several cobalt oxides and hydroxides, the main satellite peak at 786.3 eV suggests that the new phase is more likely $Co(OH)_2$ or CoO rather than a higher valent CoOOH or Co_3O_4 phase.[34,38,39] Quantitative analysis shows that the surface composition ratio of $Co^{\delta+}$ over all other Co species decreased from 4 to 0.5, indicating that approximately 60% of the Co_2P surface of the fresh sample has been oxidized during the stability test in alkaline. To assess purely chemical dissolution in a nonwired configuration, control experiments were performed by immersing fresh Co_2P@CP electrodes in both 0.5 M H_2SO_4 and 1 M KOH without applying a bias voltage for the same duration as stability

DOI: 10.1021/acsenergylett.8b00514
ACS Energy Lett. 2018, 3, 1360−1365

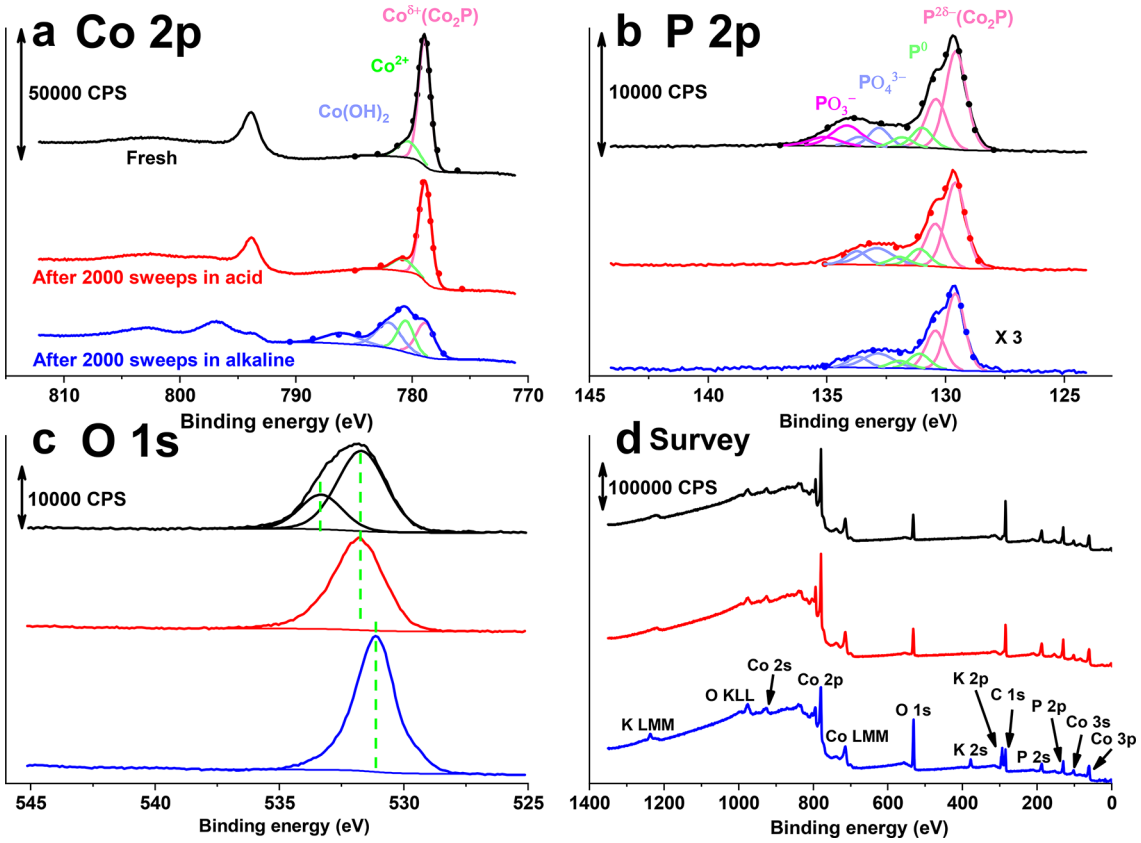

Figure 3. X-ray photoelectron spectra of the (a) Co 2p region, (b) P 2p region, and (c) O 1s region and (d) survey spectrum of fresh (black solid line) and postcatalysis Co_2P@CP in acid (red solid line) and alkaline (blue solid line).

tests (ca. 5 h). No obvious change of the Co 2p spectra (Figure S3a) could be observed between fresh and spent Co_2P@CP electrodes after prolonged immersion in both acid and alkaline electrolytes.

The P 2p XPS spectra show two main peaks at binding energies of 129.6 and 130.5 eV (ratio 2:1), corresponding to the spin−orbit split doublet of phosphide $2p_{3/2}$ and $2p_{1/2}$ lines, respectively.[16,17,27,35−37] The doublet at BE(P $2p_{3/2}$) = 131.1 eV and BE(P $2p_{1/2}$) = 131.9 eV is attributed to elementary P as a remainder from thermal phosphidization treatment.[40,41] The doublet at 132.8 and 133.6 eV and the doublet at 134.2 and 135.1 eV are attributed to orthophosphate[40−42] and metaphosphate,[40,41] respectively. The phosphate components may result from either surface oxidation upon air exposure or residues from thermal decomposition of NaH_2PO_2. The total Co to P ratio of 0.33 indicates the surface of fresh Co_2P being rich in P, which is typically observed for phosphides made by thermal phosphidization.[32] The metaphosphate species is likely water-soluble because the metaphosphate component has disappeared during both acid and alkaline stability tests as well as in the acid and alkaline immersion control experiments (Figure S3 b). No other change except the disappearance of the metaphosphate species is observed after the stability test in acid. In contrast, the XPS intensity of phosphorus decreased dramatically after the stability test in alkaline. The total Co/P ratio increased up to 1.65, although the ratios of the different phosphorus species of the sample used in alkaline are similar to those of the sample after acid electrolysis.

The O 1s spectrum of the fresh sample displays two overlapping peaks at binding energies of 531.8 and 532.3 eV, where the former one can be probably assigned to a combination of orthophosphate[42] and surface carbonate species,[43] while the latter is attributed to oxygen in the metaphosphate.[44] After stability tests in both acidic and alkaline electrolytes, the oxygen peak corresponding to metaphosphate disappears, in line with the disappearance of P 2p peaks of metaphosphate. After the stability test in alkaline, the main peak at 531.1 eV indicates the formation of a surface hydroxide,[34,38,39] which is also consistent with the Pourbaix diagram of cobalt.[45,46] The XPS survey spectra in Figure 3d rule out the possibility of Pt contamination from the counter electrode. K 2s and K 2p peaks after alkaline treatment result from the adsorption of K^+ cations from the KOH electrolyte.

The significant surface composition change after stability tests in alkaline seems to contradict the relatively stable LSV curves shown in Figure 1. The morphology changes shown in the SEM images (especially for the sample tested in alkali) (insets in Figure 2) suggest that the change of surface area during the stability tests might have contributed to the explanation of this apparent contradiction. To confirm this hypothesis, we make use of the double layer capacitance method to evaluate the ECSA of the samples.[47,48] The double layer capacitance C_{dl} was measured by scanning the potential around the open-circuit potential (OCP). The potential regions were carefully chosen to avoid interference of pseudocapacitances caused by surface redox reactions. As shown in Figures S4 and S5, the negative and positive current densities are approximately symmetric at each scan rate and the plot of log i versus scan rate is linear, where i is the geometric charging current density measured at the center of the scan range.

The ECSAs of Co_2P@CP increase by 15% after the stability test in 0.5 M H_2SO_4, while a 100% increase is observed after the

DOI: 10.1021/acsenergylett.8b00514
ACS Energy Lett. 2018, 3, 1360−1365

stability test in 1.0 M KOH. Noting that this change is not reflected in geometric current densities as used in Figure 1, the ECSA-normalized current density should be used instead as a better method of determining the real catalytic activity and stability. Figure 4a gives the polarization curves from Figure 1

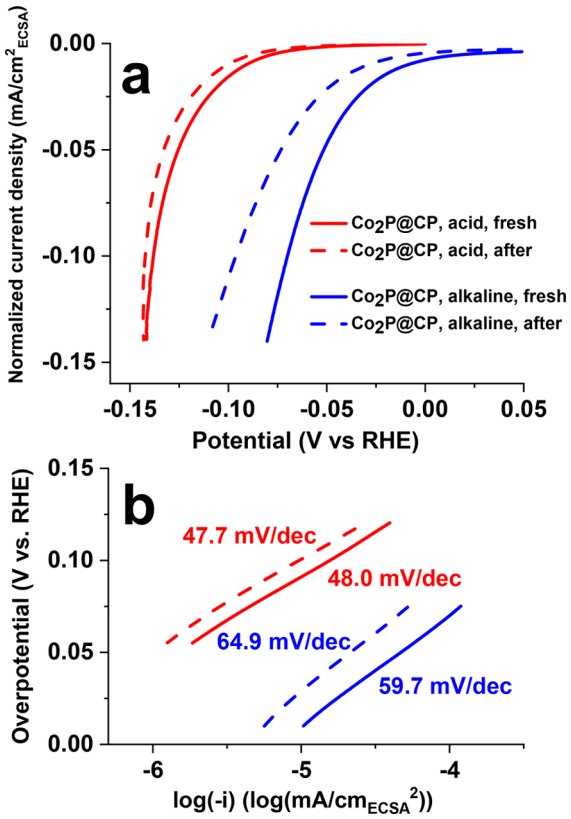

Figure 4. (a) Polarization curves (normalized by ECSA) of Co_2P@CP before (solid lines) and after 2000 LSV sweeps (dashed lines) in 0.5 M H_2SO_4 and 1 M KOH; (b) corresponding Tafel plots of Co_2P@CP before and after stability tests.

but now normalized to ECSA. The activity loss of Co_2P@CP in acidic electrolyte is minor due to the minor ECSA change before and after the stability test. Tafel slopes remain unchanged (ca. 48 mV/dec in Figure 4 b), and the exchange current density (j_0) decreases from 1.25×10^{-7} to 7.94×10^{-8} mA/cm$^2_{ECSA}$ after the stability test. Meanwhile, significant activity loss is observed in alkaline solution due to a striking increase of ECSA after the stability test. The overpotential required to achieve 0.1 mA/cm$_{ECSA}^2$ current density increased from 70 to 96 mV after the stability test. Tafel slopes increased from 59.7 to 64.9 mV/dec, and j_0 decreases from 6.31×10^{-6} to 3.72×10^{-6} mA/cm$^2_{ECSA}$ after the stability test.

The electrolytes after stability tests and control immersion experiments were collected and analyzed by ICP-OES (Figure 5). After the stability test in acidic electrolyte (volume: 25 mL), the concentrations of dissolved Co and P per mg of Co_2P@CP were determined to be 25.7 ± 4.0 and 12.0 ± 1.9 μmol/L, respectively. The control immersion experiment shows concentrations of Co and P of 18.5 ± 1.5 and 5.6 ± 0.3 μmol/L, respectively. Although the concentrations of both Co and P in the immersion experiment are lower than those after the stability test, chemical dissolution contributes significantly to Co_2P degradation in acid. In alkaline electrolyte, the degradation mechanism of Co_2P is completely different. The

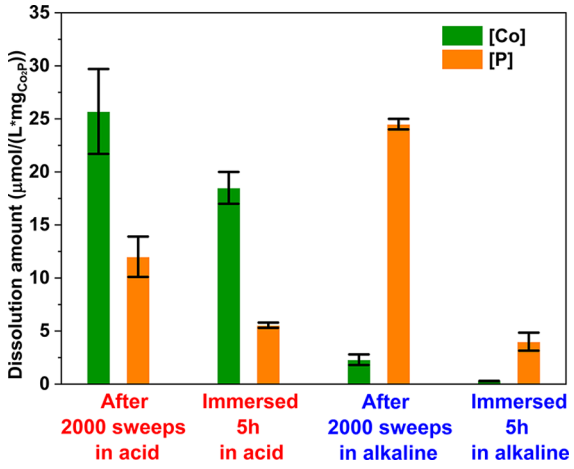

Figure 5. ICP-OES analysis of Co and P ion dissolution concentration in the electrolyte during the stability tests and the corresponding nonelectrochemical control immersion experiments.

concentration of phosphorus (24.5 ± 0.5 μmol/L) is much higher than that of cobalt (2.3 ± 0.5 μmol/L) after the stability test in alkaline because of the very low solubility of oxidic cobalt species in alkaline solutions. For the control immersion experiment, the leaching concentrations of both species are much lower, with 0.28 ± 0.02 μmol/L for Co and 4.0 ± 0.9 μmol/L for P, as compared with those after the stability test. With this, we conclude that Co_2P degradation in alkaline is mainly induced by the LSV sweeps. The stability of non-noble-metal-based electrocatalysts in acid has been elaborately studied by monitoring the concentration of metal ions with online ICP-MS.[49] The conclusion is that the nonmetal materials are stable at HER potentials but dissolve substantially at OCP. However, merely monitoring the leaching concentration of metal ions and assuming stoichiometric dissolution of nonmetal elements is not sufficient when assessing the stability of electrocatalysts in alkaline solutions. As we show here, P is preferentially leached out of the film, and Co turns to hydroxide.[50]

In order to increase the apparent activity of earth-abundant electrocatalysts, a large amount of materials is usually loaded on a porous conductive substrate such as CP or metal foam. However, caution should be exercised in electrochemical stability testing. First, the possible variation of ECSA during the stability test is often ignored. In the case of Co_2P@CP, the ECSA increases by a factor of 2 after 2000 LSV sweeps in alkaline electrolyte. This change is overlooked if the current density is normalized by either the geometric area or mass of the electrode or if only the ECSA before testing is used. Second, surface-sensitive characterization methods are mandatory to assess the occurring surface chemistry changes. Although no new phase of Co_2P is observed by XRD and Raman after stability tests in alkaline, significant surface composition changes have been illustrated in XPS. Third, high catalyst loadings may result in artificially prolonged lifetimes. Therefore, analyzing the composition of the electrolytes after the electrochemical test is critical.

In conclusion, we evaluated the stability of Co_2P, made by thermal phosphidization, as HER electrocatalyst in both acidic and alkaline electrolytes. With detailed electrochemical and spectroscopic characterization before and after stability testing, we conclude that Co_2P degradation follows two different routes in acid and alkaline. In acid, both Co and P dissolve, but the remaining exposed Co_2P surface is still active for HER. In

DOI: 10.1021/acsenergylett.8b00514
ACS Energy Lett. 2018, 3, 1360−1365

alkaline, P is preferentially dissolved while the remaining cobalt on the surface turns to hydroxide and the HER activity decreases accordingly. We note that TMPs prepared by different methods may have different dissolution mechanisms. However, on the basis of our results, we stress that the constancy of current−potential curves alone during the stability test does not unambiguously confirm electrode stability. Only comprehensive postcatalysis structural and compositional analysis of both the electrode and electrolyte could reflect the intrinsic stability, as well as the degradation mechanism of earth-abundant electrocatalysts.

■ ASSOCIATED CONTENT

Supporting Information

The Supporting Information is available free of charge on the ACS Publications website at DOI: 10.1021/acsenergylett.8b00514.

Experimental details, further materials characterization (X-ray diffraction, Raman spectroscopy, X-ray photoelectron spectroscopy, double layer capacitance measurements), and details on calculations of the electrochemically active surface area (ECSA) (PDF)

■ AUTHOR INFORMATION

Corresponding Authors

*E-mail: E.J.M.Hensen@tue.nl (E.J.M.H.).
*E-mail: J.P.Hofmann@tue.nl (J.P.H.).

ORCID

Emiel J. M. Hensen: 0000-0002-9754-2417
Jan P. Hofmann: 0000-0002-5765-1096

Author Contributions

†Y.Z. and L.G. contributed equally to the work.

Notes

The authors declare no competing financial interest.

■ ACKNOWLEDGMENTS

The authors like to thank Dr. Andrey Goryachev, Dr. Freddy E. Oropeza, and Longfei Wu (Eindhoven University of Technology) for fruitful discussions. Akhil Sharma (Eindhoven University of Technology) is thanked for assistance in Raman spectroscopy measurements. Y.Z. acknowledges financial support from the China Scholarship Council (CSC). L.G. and E.J.M.H. acknowledge funding by an NWO Vici grant.

■ REFERENCES

(1) Vesborg, P. C. K.; Seger, B.; Chorkendorff, I. Recent Development in Hydrogen Evolution Reaction Catalysts and Their Practical Implementation. *J. Phys. Chem. Lett.* **2015**, *6*, 951−957.

(2) Zeng, M.; Li, Y. Recent Advances in Heterogeneous Electrocatalysts for the Hydrogen Evolution Reaction. *J. Mater. Chem. A* **2015**, *3*, 14942−14962.

(3) Morales-Guio, C. G.; Stern, L.; Hu, X. Nanostructured Hydrotreating Catalysts for Electrochemical Hydrogen Evolution. *Chem. Soc. Rev.* **2014**, *43*, 6555−6569.

(4) Anantharaj, S.; Ede, S. R.; Sakthikumar, K.; Karthick, K.; Mishra, S.; Kundu, S. Recent Trends and Perspectives in Electrochemical Water Splitting with an Emphasis to Sulphide, Selenide and Phosphide Catalysts of Fe, Co and Ni: A Review. *ACS Catal.* **2016**, *6*, 8069−8097.

(5) Pu, Z.; Liu, Q.; Asiri, A. M.; Luo, Y.; Sun, X.; He, Y. 3D Macroporous MoS_2 thin Film: In Situ Hydrothermal Preparation and Application as a Highly Active Hydrogen Evolution Electrocatalyst at All pH Values. *Electrochim. Acta* **2015**, *168*, 133−138.

(6) Popczun, E. J.; McKone, J. R.; Read, C. G.; Biacchi, A. J.; Wiltrout, A. M.; Lewis, N. S.; Schaak, R. E. Nanostructured Nickel Phosphide as an Electrocatalyst for the Hydrogen Evolution Reaction. *J. Am. Chem. Soc.* **2013**, *135*, 9267−9270.

(7) Laursen, A. B.; Patraju, K. R.; Whitaker, M. J.; Retuerto, M.; Sarkar, T.; Yao, N.; Ramanujachary, K. V.; Greenblatt, M.; Dismukes, G. C. Nanocrystalline Ni_5P_4 : A Hydrogen Evolution Electrocatalyst of Exceptional Efficiency in Both Alkaline and Acidic Media. *Energy Environ. Sci.* **2015**, *8*, 1027−1034.

(8) Huang, Z.; Chen, Z. Z.; Chen, Z. Z.; Lv, C.; Meng, H.; Zhang, C. $Ni_{12}P_5$ Nanoparticles as an Efficient Catalyst for Hydrogen Generation via Electrolysis and Photoelectrolysis. *ACS Nano* **2014**, *8*, 8121−8129.

(9) Liu, Q.; Tian, J.; Cui, W.; Jiang, P.; Cheng, N.; Asiri, A. M.; Sun, X. Carbon Nanotubes Decorated with CoP Nanocrystals: A Highly Active Non-Noble-Metal Nanohybrid Electrocatalyst for Hydrogen Evolution. *Angew. Chem., Int. Ed.* **2014**, *53*, 6710−6714.

(10) Popczun, E. J.; Read, C. G.; Roske, C. W.; Lewis, N. S.; Schaak, R. E. Highly Active Electrocatalysis of the Hydrogen Evolution Reaction by Cobalt Phosphide Nanoparticles. *Angew. Chem., Int. Ed.* **2014**, *53*, 5427−5430.

(11) Jiang, N.; You, B.; Sheng, M.; Sun, Y. Electrodeposited Cobalt-Phosphorous-Derived Films as Competent Bifunctional Catalysts for Overall Water Splitting. *Angew. Chem., Int. Ed.* **2015**, *54*, 6251−6254.

(12) Huang, Z.; Chen, Z.; Chen, Z.; Lv, C.; Humphrey, M. G.; Zhang, C. Cobalt Phosphide Nanorods as an Efficient Electrocatalyst for the Hydrogen Evolution Reaction. *Nano Energy* **2014**, *9*, 373−382.

(13) Saadi, F. H.; Carim, A. I.; Verlage, E.; Hemminger, J. C.; Lewis, N. S.; Soriaga, M. P. CoP as an Acid-Stable Active Electrocatalyst for the Hydrogen-Evolution Reaction: Electrochemical Synthesis, Interfacial Characterization and Performance Evaluation. *J. Phys. Chem. C* **2014**, *118*, 29294−29300.

(14) Saadi, F. H.; Carim, A. I.; Drisdell, W. S.; Gul, S.; Baricuatro, J. H.; Yano, J.; Soriaga, M. P.; Lewis, N. S. Operando Spectroscopic Analysis of CoP Films Electrocatalyzing the Hydrogen-Evolution Reaction. *J. Am. Chem. Soc.* **2017**, *139*, 12927−12930.

(15) Tian, J.; Liu, Q.; Asiri, A. M.; Sun, X. Self-Supported Nanoporous Cobalt Phosphide Nanowire Arrays: An Efficient 3D Hydrogen-Evolving Cathode over the Wide Range of pH 0−14. *J. Am. Chem. Soc.* **2014**, *136* (21), 7587−7590.

(16) Liu, T.; Xie, L.; Yang, J.; Kong, R.; Du, G.; Asiri, A. M.; Sun, X.; Chen, L. Self-Standing CoP Nanosheets Array: A Three-Dimensional Bifunctional Catalyst Electrode for Overall Water Splitting in Both Neutral and Alkaline Media. *ChemElectroChem* **2017**, *4* (8), 1840−1845.

(17) Xiong, X.; Ji, Y.; Xie, M.; You, C.; Yang, L.; Liu, Z.; Asiri, A. M.; Sun, X. MnO_2-CoP_3 nanowires Array: An Efficient Electrocatalyst for Alkaline Oxygen Evolution Reaction with Enhanced Activity. *Electrochem. Commun.* **2018**, *86*, 161−165.

(18) Xu, Y.; Wu, R.; Zhang, J.; Shi, Y.; Zhang, B. Anion-Exchange Synthesis of Nanoporous FeP Nanosheets as Electrocatalysts for Hydrogen Evolution Reaction. *Chem. Commun.* **2013**, *49*, 6656−6658.

(19) Jiang, P.; Liu, Q.; Liang, Y.; Tian, J.; Asiri, A. M.; Sun, X. A Cost-Effective 3D Hydrogen Evolution Cathode with High Catalytic Activity: FeP Nanowire Array as the Active Phase. *Angew. Chem., Int. Ed.* **2014**, *53*, 12855−12859.

(20) Callejas, J. F.; McEnaney, J. M.; Read, C. G.; Crompton, J. C.; Biacchi, A. J.; Popczun, E. J.; Gordon, T. R.; Lewis, N. S.; Schaak, R. E. Electrocatalytic and Photocatalytic Hydrogen Production from Acidic and Neutral-pH Aqueous Solutions Using Iron Phosphide Nanoparticles. *ACS Nano* **2014**, *8*, 11101−11107.

(21) Huang, Z.; Chen, Z.; Chen, Z.; Lv, C.; Humphrey, M. G.; Zhang, C. Molybdenum Phosphide as an Efficient Electrocatalyst for the Hydrogen Evolution Reaction. *Nano Energy* **2014**, *9*, 373−382.

(22) Xing, Z.; Liu, Q.; Asiri, A. M.; Sun, X. Closely Interconnected Network of Molybdenum Phosphide Nanoparticles: A Highly Efficient Electrocatalyst for Generating Hydrogen from Water. *Adv. Mater.* **2014**, *26*, 5702−5707.

DOI: 10.1021/acsenergylett.8b00514
ACS Energy Lett. 2018, 3, 1360−1365

(23) Kibsgaard, J.; Jaramillo, T. F. Molybdenum Phosphosulfide: An Active, Acid-Stable, Earth- Abundant Catalyst for the Hydrogen Evolution Reaction. *Angew. Chem., Int. Ed.* **2014**, *53*, 14433−14437.
(24) McEnaney, J. M.; Chance Crompton, J.; Callejas, J. F.; Popczun, E. J.; Read, C. G.; Lewis, N. S.; Schaak, R. E. Electrocatalytic Hydrogen Evolution Using Amorphous Tungsten Phosphide Nanoparticles. *Chem. Commun.* **2014**, *50*, 11026−11028.
(25) Pu, Z.; Liu, Q.; Asiri, A. M.; Sun, X. Tungsten Phosphide Nanorod Arrays Directly Grown on Carbon Cloth: A Highly Efficient and Stable Hydrogen Evolution Cathode at All pH Values. *ACS Appl. Mater. Interfaces* **2014**, *6*, 21874−21879.
(26) Tian, J.; Liu, Q.; Cheng, N.; Asiri, A. M.; Sun, X. Self-Supported Cu_3P Nanowire Arrays as an Integrated High-Performance Three-Dimensional Cathode for Generating Hydrogen from Water. *Angew. Chem., Int. Ed.* **2014**, *53*, 9577−9581.
(27) Kibsgaard, J.; Tsai, C.; Chan, K.; Benck, J. D.; Nørskov, J. K.; Abild-Pedersen, F.; Jaramillo, T. F. Designing an Improved Transition Metal Phosphide Catalyst for Hydrogen Evolution Using Experimental and Theoretical Trends. *Energy Environ. Sci.* **2015**, *8*, 3022−3029.
(28) Hao, J.; Yang, W.; Zhang, Z.; Tang, J. Metal−organic Frameworks Derived $Co_xFe_{1-x}P$ Nanocubes for Electrochemical Hydrogen Evolution. *Nanoscale* **2015**, *7*, 11055−11062.
(29) Li, Y.; Zhang, H.; Jiang, M.; Kuang, Y.; Sun, X.; Duan, X. Ternary NiCoP Nanosheet Arrays: An Excellent Bifunctional Catalyst for Alkaline Overall Water Splitting. *Nano Res.* **2016**, *9*, 2251−2259.
(30) Frydendal, R.; Paoli, E. A.; Knudsen, B. P.; Wickman, B.; Malacrida, P.; Stephens, I. E. L.; Chorkendorff, I. Benchmarking the Stability of Oxygen Evolution Reaction Catalysts: The Importance of Monitoring Mass Losses. *ChemElectroChem* **2014**, *1*, 2075−2081.
(31) Jiao, L.; Zhou, Y.-X.; Jiang, H.-L. Metal−organic Framework-Based CoP/reduced Graphene Oxide: High-Performance Bifunctional Electrocatalyst for Overall Water Splitting. *Chem. Sci.* **2016**, *7*, 1690−1695.
(32) Goryachev, A.; Gao, L.; Zhang, Y.; Rohling, R. Y.; Vervuurt, R. H. J.; Bol, A. A.; Hofmann, J. P.; Hensen, E. J. M. Stability of CoP_x Electrocatalysts in Continuous and Interrupted Acidic Electrolysis of Water. *ChemElectroChem* **2018**, *5*, 1230−1239.
(33) Callejas, J. F.; Read, C. G.; Popczun, E. J.; McEnaney, J. M.; Schaak, R. E. Nanostructured Co_2P Electrocatalyst for the Hydrogen Evolution Reaction and Direct Comparison with Morphologically Equivalent CoP. *Chem. Mater.* **2015**, *27*, 3769−3774.
(34) Yang, J.; Liu, H.; Martens, W. N.; Frost, R. L. Synthesis and Characterization of Cobalt Hydroxide, Cobalt Oxyhydroxide, and Cobalt Oxide Nanodiscs. *J. Phys. Chem. C* **2010**, *114*, 111−119.
(35) Grosvenor, A. P.; Wik, S. D.; Cavell, R. G.; Mar, A. Examination of the Bonding in Binary Transition-Metal Monophosphides MP (M = Cr, Mn, Fe, Co) by X-Ray Photoelectron Spectroscopy. *Inorg. Chem.* **2005**, *44*, 8988−8998.
(36) Diplas, S.; Prytz; Karlsen, O. B.; Watts, J. F.; Taftø, J. A Quantitative Study of Valence Electron Transfer in the Skutterudite Compound CoP_3 by Combining X-Ray Induced Auger and Photoelectron Spectroscopy. *J. Phys.: Condens. Matter* **2007**, *19*, 246216.
(37) Cao, S.; Chen, Y.; Hou, C.-C.; Lv, X.-J.; Fu, W.-F. Cobalt Phosphide as a Highly Active Non-Precious Metal Cocatalyst for Photocatalytic Hydrogen Production under Visible Light Irradiation. *J. Mater. Chem. A* **2015**, *3*, 6096−6101.
(38) Tan, B. J.; Klabunde, K. J.; Sherwood, P. M. A. XPS Studies of Solvated Metal Atom Dispersed Catalysts. Evidence for Layered Cobalt—Manganese Particles on Alumina and Silica. *J. Am. Chem. Soc.* **1991**, *113*, 855−861.
(39) Biesinger, M. C.; Payne, B. P.; Grosvenor, A. P.; Lau, L. W. M.; Gerson, A. R.; Smart, R. S. C. Resolving Surface Chemical States in XPS Analysis of First Row Transition Metals, Oxides and Hydroxides: Cr, Mn, Fe, Co and Ni. *Appl. Surf. Sci.* **2011**, *257*, 2717−2730.
(40) Franke, R.; Chassé, T.; Streubel, P.; Meisel, A. Auger Parameters and Relaxation Energies of Phosphorus in Solid Compounds. *J. Electron Spectrosc. Relat. Phenom.* **1991**, *56*, 381−388.
(41) Pelavin, M.; Hendrickson, D. N.; Hollander, J. M.; Jolly, W. L. Phosphorus 2p Electron Binding Energies. Correlation with Extended Hückel Charges. *J. Phys. Chem.* **1970**, *74*, 1116−1121.
(42) Morgan, W. E.; Van Wazer, J. R.; Stec, W. J. Inner-Orbital Photoelectron Spectroscopy of the Alkali Metal Halides, Perchlorates, Phosphates, and Pyrophosphates. *J. Am. Chem. Soc.* **1973**, *95*, 751−755.
(43) Stoch, J.; Gablankowska-Kukucz, J. The Effect of Carbonate Contaminations on the XPS O 1s Band Structure in Metal Oxides. *Surf. Interface Anal.* **1991**, *17*, 165−167.
(44) Gresch, R.; Muller-Warmuth, W.; Dutz, H. X-Ray Photoelectron Spectroscopy of Sodium Phosphate Glasses. *J. Non-Cryst. Solids* **1979**, *34*, 127−136.
(45) Bajdich, M.; García-Mota, M.; Vojvodic, A.; Nørskov, J. K.; Bell, A. T. Theoretical Investigation of the Activity of Cobalt Oxides for the Electrochemical Oxidation of Water. *J. Am. Chem. Soc.* **2013**, *135* (36), 13521−13530.
(46) Gerken, J. B.; McAlpin, J. G.; Chen, J. Y. C.; Rigsby, M. L.; Casey, W. H.; Britt, R. D.; Stahl, S. S. Electrochemical Water Oxidation with Cobalt-Based Electrocatalysts from PH 0−14: The Thermodynamic Basis for Catalyst Structure, Stability, and Activity. *J. Am. Chem. Soc.* **2011**, *133* (36), 14431−14442.
(47) McCrory, C. C. L.; Jung, S.; Peters, J. C.; Jaramillo, T. F. Benchmarking Heterogeneous Electrocatalysts for the Oxygen Evolution Reaction. *J. Am. Chem. Soc.* **2013**, *135*, 16977−16987.
(48) Trasatti, S.; Petrii, O. A. Real Surface Area Measurements in Electrochemistry. *J. Electroanal. Chem.* **1992**, *327*, 353−376.
(49) Ledendecker, M.; Mondschein, J. S.; Kasian, O.; Geiger, S.; Göhl, D.; Schalenbach, M.; Zeradjanin, A.; Cherevko, S.; Schaak, R. E.; Mayrhofer, K. Stability and Activity of Non-Noble-Metal-Based Catalysts Toward the Hydrogen Evolution Reaction. *Angew. Chem., Int. Ed.* **2017**, *56*, 9767−9771.
(50) Costa, J. D.; Lado, J. L.; Carbó-Argibay, E.; Paz, E.; Gallo, J.; Cerqueira, M. F.; Rodríguez-Abreu, C.; Kovnir, K.; Kolen'ko, Y. V. Electrocatalytic Performance and Stability of Nanostructured Fe-Ni Pyrite-Type Diphosphide Catalyst Supported on Carbon Paper. *J. Phys. Chem. C* **2016**, *120*, 16537−16544.

DOI: 10.1021/acsenergylett.8b00514
ACS Energy Lett. 2018, 3, 1360−1365